Research Article

Ultrasound-Assisted Biomimetic Synthesis of MOF-Hap Nanocomposite via 10xSBF-Like for the Photocatalytic Degradation of Metformin

Mark Tristan D.C. Español, ER Joshua G. Garcia, Louise Andrea V. Maligaya, Carla Mae S. Santos, Jan Abigail H. Santos, Nemia G. Suarnaba and Rugi Vicente C. Rubi*
Department of Chemical Engineering, College of Engineering, Adamson University, Manila, Philippines

Reibelle Raguindin
Hanyang University, Seoul, South Korea

* Corresponding author. E-mail: rugi.vicente.rubi@adamson.edu.ph DOI: 10.14416/j.asep.2023.11.002
Received: 18 July 2023; Revised: 28 August 2023; Accepted: 20 September 2023; Published online: 9 November 2023

Abstract
High levels of emerging pollutants, such as pharmaceutical compounds like metformin (MET), have been an issue for many years. The effective removal of these compounds from wastewater poses a significant challenge and has spurred interest among researchers. This study aims to integrate two of the prominent research interests in photocatalysis, Metal-Organic Frameworks (MOF), and Hydroxyapatite (HAp), and tests their effectiveness in the photocatalytic degradation of MET. The MOF-HAp was produced using a biomimetic method via 10xSBF-like solution with and without ultrasound assistance at varying biomimetic times. MOF-HAp nanocomposite's photocatalytic degradation capabilities were tested by degrading MET, considering varying parameters – initial pollutant concentration, catalyst loading, and exposure time. Results showed that a biomimetic time of 6 h synthesized with ultrasound irradiation presented the most promising physicochemical properties for MOF-HAp, as verified by the X-ray Fluorescence (XRF), Scanning Electron Microscope (SEM), Brunauer-Emmett-Teller (BET), X-ray Diffractometer (XRD), and Fourier Transform Infrared Spectroscopy (FTIR) analyses. In the photocatalytic degradation of MET, catalyst loading, exposure time, and initial pollutant concentration were found to have significant effects on the percent degradation. The initial concentration of 8 ppm, catalyst loading of 0.25 g, and 120 min of exposure time produced the highest percent degradation with an average of 82.25%. The findings of this study prove MOF-HAp's potential to effectively degrade organic and pharmaceutical pollutants in wastewater.

Keywords: 10xSBF-like solution, Biomimetic method, Hydroxyapatite, Metal-organic frameworks, Metformin, Photocatalytic degradation, Ultrasound

1 Introduction

Pharmaceuticals and personal care products (PPCPs) are a class of emerging environmental chemical pollutants distinguished by their bioactivity and high solubility that can cause health complications to humans and other living organisms. Moreover, pharmaceutical products enter the water system as wastewater that reaches the surface and groundwater [1].

One of the most widely used pharmaceutical products is metformin (MET). MET (C4H11N5) is the most commonly used anti-hyperglycemic agent to treat non-insulin-dependent diabetes mellitus (NIDDM) or type II diabetes mellitus [2]. This medication is also an anti-cancer agent and a treatment for women who have polycystic ovary syndrome [3]. It is one of the many chemical wastes that are abundant in the environment. Traces of MET, which is excreted by humans without being fully metabolized (about 70% in urine and 30% in feces), has been identified in wastewater treatment

facilities as well as various water systems. This presence is attributed to the significant quantities prescribed to individuals (ranging from 500–2,000 mg per person per day). In wastewater, MET levels ranging from 20–94 μg/L have been observed and surface/groundwater samples have revealed concentrations as high as 1,700 ng/L [4].

Advanced Oxidation Processes (AOPs) are successful ways of treating PPCPs and this also includes photocatalytic degradation. Photocatalytic degradation includes hydroxyl radicals from the pollutants responsible for the mineralization process. Further mineralization of the intermediates results in less persistent and more biodegradable organics by-products [5], [6].

The use of photocatalysis has displayed considerable potential as an economical, environmentally conscious, and sustainable approach for treating water and wastewater. The efficiency of this innovative oxidation method in eradicating enduring organic pollutants and microorganisms from wastewater has been extensively validated. However, the employment of photocatalysis systems for water treatment encounters a range of restrictions that necessitate further exploration [1], [6]. The treatment of organic compounds often involves photocatalytic degradation and metallic oxides, namely titanium oxide (TiO_2), cerium oxide (CeO_2), zinc oxide (ZnO), zirconium oxide (ZrO_2), manganese oxide (MnO_2), and tin oxide (SnO_2), are regarded as exceptional photocatalysts within this classification due to their capacity for maintaining stability across a broad pH spectrum, heightened efficiency, affordability, widespread accessibility, minimal toxicity, environmentally friendly characteristics, and the production of highly oxidative photo-induced holes. However, there are several drawbacks associated with the application of these metal oxides in the process of photocatalytic degradation. These downsides include incomplete mineralization and a wide band gap, factors that considerably constrain their effectiveness in promoting photocatalytic activity [7].

Hydroxyapatite (HAp) and Metal-Organic Frameworks (MOF) are some of the emerging research interests with numerous applications, including photocatalytic degradation. HAp is the primary component of natural bone that was developed to be used in biomedical applications. A study conducted by Reddy *et al.*, [8] showed that HAp was used in the photocatalytic degradation of calmagite, an azo dye, in aqueous suspension. It was used because of its great sorption properties. Moreover, it is considered a novel stable biomaterial for heterogeneous photocatalytic degradation of pollutants. On the other hand, MOF materials, in general, are widely used as photocatalysts due to their highly tunable bandgap and their huge compositional and structural versatility. MOF's versatility can be observed in its physicochemical aspects such as porosity, structures, and compositions [9]. Moreover, they have been recently employed as photocatalysts to oxidize various pollutants due to their immense porosity, high surface area, and facile preparation [9], [10].

Studies on integrating ultrasound in the synthesis of nanocomposites HAp have gained extensive interest because of the advantages that it provides on the produced photocatalysts. It has been reported that ultrasound-assisted reactions in the synthesis of composites are helpful because they can give significant oxidation properties, high yield, enhanced kinetics, and addition of molecules. Moreover, this method can influence the intermolecular addition and stability of composites due to ultrasonic cavitations [11]. The use of ultrasound to assist the reaction can reduce the surface area of the synthesized composite. Also, the quantity of pollutants that can be absorbed by the composite is higher when it is synthesized by an ultrasound-assisted method [12].

The combination of HAp and MOFs in photocatalysis provides various advantages for specific applications. Both HAp and MOFs have their limitations, with MOFs exhibiting insufficient utilization of visible light, which hampers their photocatalytic activity. Additionally, MOFs suffer from rapid recombination of photogenerated carriers [13]. On the other hand, HAp is a stable biomaterial that performs well under UV irradiation and is commonly used in photocatalysis [8]. By combining HAp and MOFs, synergistic effects occur as the unique properties of each material complement each other, resulting in improved photocatalytic performance. HAp enhances stability and biocompatibility, while MOFs contribute to increased light absorption and charge carrier separation.

Against the background provided, this work has facilitated the ultrasound-assisted biomimetic synthesis of MOF-HAp nanocomposite using 10xSBF-like and

investigated its potential in the photocatalytic degradation of MET. The 10xSBF-like solution provides a simple, rapid, and efficient production of HAp while also preventing the formation of giant crystals [14]. Moreover, the effects of parameters such as catalyst loading, exposure time, and pollutant concentration, on the degradation were systematically investigated.

To the best of our knowledge, the in situ formation of the MOF-HAp nanocomposite in 10xSBF-like solution with ultrasound irradiation and its use in the photocatalytic degradation of metformin has not yet been reported. This work has launched potential applications of nanocomposites in environmental remediation and pharmaceutical waste management, particularly in MET contamination.

2 Materials and Methods

2.1 *Chemicals and reagents*

In this study, MOF or MIL-100 was produced using the following: Reagent Plus, 98% $FeCl_2 \cdot 4H_2O$, 95% H3BTC, deionized and distilled water, and AR (analytical reagent) grade NaOH.

For the 10xSBF-like solution, the protocol preparation was adapted based on the work of Demirtas *et al.* [14], which is composed of the following analytical grade reagent (AR): NaCl, $NaHCO_3$, KCl, $Na_2HPO_4 \cdot H_2O$, $MgCl_2 \cdot 6H_2O$, $CaCl_2 \cdot H_2O$, and deionized water, to promote the growth of HAp and to form the MOF-HAp photocatalyst nanocomposite. The pollutant MET ($C_4H_{11}N_5$) with pharmaceutical standard was purchased from Sigma-Aldrich, Singapore.

2.2 *Experimental set-up*

Shown in Figure 1 is the self-fabricated reactor which is composed of (a) five UV lamps (13W, λmax = 460 nm), which serve as the light source, and (b) one exhaust fan installed at the back of the reactor to maintain the room temperature of the system. Silver wrappers cover the inside of the reactor to ensure an equal distribution of light during the photocatalytic process. Moreover, there are (c) two magnetic stirrers with (d) two magnetic stir bars constructed in the reactor, which were occupied by (e) two 250 mL beakers filled with MET solution and photocatalyst during the photocatalytic degradation.

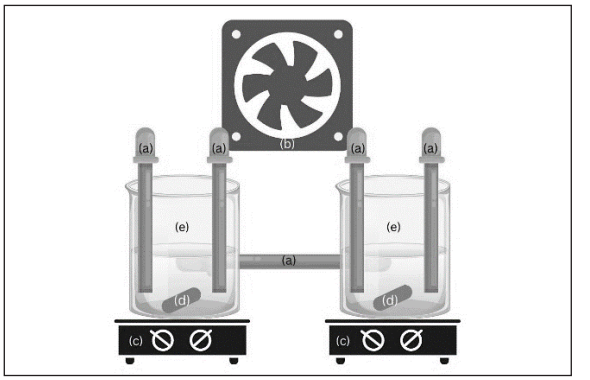

Figure 1: Photocatalytic reactor's diagram.

2.3 *MOF synthesis*

The MIL-100 (Fe) was synthesized based on the procedure discussed in the work of Guesh *et al.*, [9]. Two solutions were prepared; the first solution contained 11.732 g of H3BTC dissolved in 6.384 g of 1 M NaOH aqueous solution. The second solution was prepared by dissolving 15.82 g of $FeCl_2 \cdot 4H_2O$ in 680.4 mL of H_2O. The two solutions were mixed using a magnetic stirrer, then after becoming a homogeneous solution in both cases, the first solution was added dropwise over the second while stirring which continued for 24 h at room temperature. The solid and liquid parts were separated by centrifugation at 4000 rpm and then washed twice with deionized water and once with ethanol; the recovered solid is MIL-100 (Fe). The sample was dried using the freeze dryer available at the Instrumentation and Process Control (IPC) Laboratory at Adamson University. The powder was collected, labeled as MOF, ground by using a nutrient extractor, and weighed to yield 18.8313 g.

2.4 *Preparation of 10xSBF-like solution*

The SBF solution to be used in this study will be the 10xSBF-like solution, which contains a lower concentration of phosphate ions than that of 10xSBF. The 10xSBF-like solution was prepared in reference to the previous formulation by Demirtaş *et al.* [14].

The chemical reagents required to produce the 10xSBF-like solution were NaCl (58.443 g), KCl (0.373 g), $CaCl_2 \cdot 2H_2O$ (2.774), $MgCl_2 \cdot 6H_2O$ (1.016), and $NaH_2PO4 \cdot H_2O$ (0.2174), which were added successively in 900 mL deionized water in a

glass volumetric flask and stirred magnetically at room temperature. The complete dissolution of each chemical reagent was noted before the addition of the next one. The precipitating agent for the formation of HAp, $NaHCO_3$ (0.084 g), will be added later on in the process. The aqueous stock solution will be formulated up to 1000 mL with deionized water and can be stored in a refrigerator at 4 °C. The process will be repeated to obtain sufficient volume for the preparation of MOF-HAp nanocomposite.

2.5 *Preparation of MOF-HAp nanocomposite*

Initially, 100 mL of the stock solution was prepared in four 250 mL flasks. $NaHCO_3$ (0.084g) was added to each solution to increase the ion concentration of hydrogen carbonate (HCO_3^-) to 10 mM under continuous stirring. 1 g of MOF was immersed in the solution as HAp and precipitated for 3 and 6 h, separately. The process was done both with ultrasound irradiation in an ultrasonic cleaner (Biobase) and without within an orbital shaking water bath. The produced nanocomposite was dried using the freeze dryer and the powder collected was ground using a nutrient extractor. All the equipment mentioned was available at the Instrumentation and Process Control (IPC) Laboratory at Adamson University.

2.5 *MOF-HAp characterization*

The MOF-HAp sample powder was analyzed to determine its characteristics. The elemental compositions of the nanocomposite were analyzed by X-ray Fluorescence (XRF) (Horiba Mesa 50) with the following specifications: voltage at 50 kV, filter ranging from low to mid, and a measuring time of 100 s. The surface morphology microscopic and particle sizes of the MOF-HAp nanocomposite produced were characterized by Scanning Electron Microscopy (SEM) (Apreo S Hivac). Moreover, the surface area, pore volume, and diameter of the nanocomposite were characterized by Brunauer-Emmett-Teller (BET) (BELSORP-mini II instrument (Bel Japan Inc., Japan)). The crystalline frameworks and structures of the produced MOF-HAp nanocomposite were analyzed using an X-ray diffractometer (XRD) (D8 ADVANCE- Bruker) with CuKα radiation from 10–90° at a rate of 3° per minute. Lastly, Fourier Transform Infrared Spectroscopy (FTIR) (Spectrum Two-Perkin Elmer) was used to identify the functional groups present in the sample produced.

2.7 *Photocatalytic degradation of MET*

The photocatalytic degradation of MET started with the production of MET stock solution. The formulation was based on the recent works of Aseman Bashiz and Sayyaf [15]. The MET stock solution (100 mg/L) was prepared by dissolving 100 mg of pure MET powder in 1 L of distilled water. From the stock solution, different concentrations: 8 and 12 ppm, were produced to be used in the photocatalytic degradation process. Moreover, it is advised to store the stock solution at 4 °C darkness to prevent the concentration from fluctuating.

Proceeding to the photocatalytic degradation of MET, 250 mL beakers were filled with 200 mL of MET solutions to be degraded, and varying photocatalysts were used. The prepared mixture's pH was adjusted to 7.6 with the use of 0.1 M NaOH solution and 0.1 M HCl solution. H_2O_2 was used as an oxidant in the degradation at a concentration of 7 mM to produce hydroxyl radicals. Furthermore, the mixture was mixed in the dark for 30 min before it was exposed to five UV lights (13 W, λmax = 460 nm). The variations of photocatalysts were MIL-100 only, HAp only, MOF-Hap nanocomposites, and no photocatalyst. After the photocatalytic degradation, the samples underwent filtration before being analyzed using an Ultraviolet Visible Spectrophotometer (UV-Vis) (Perkin Elmer Lambda 25) where its absorbance was red at 300–200 nm to investigate MET's concentration which was observed to be at 232 nm.

2.7.1 Degradation efficiency of MET

The initial and final concentrations of MET that will be obtained during and after the degradation process will be analyzed using UV-Vis spectroscopy. The degradation efficiency of MET can be computed using Equation (1).

$$\textit{MET removal efficiency}\ (\%) = \frac{C_0 - C_e}{C_0} \times 100 \qquad (1)$$

Where C_0 is the initial concentration of MET in the process (mg/L) and C_e is the remaining concentration of MET after the degradation process (mg/L) [15].

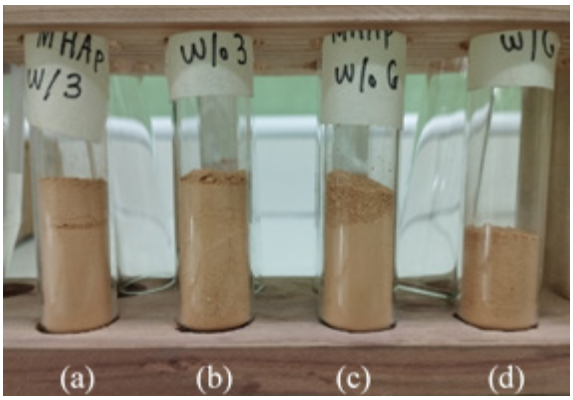

Figure 2: Synthesized MOF-HAp nanocomposites: (a) MOF-HAp$_{U3}$, (b) MOF-HAp$_{N3}$, (c) MOF-HAp$_{N6}$, and (d) MOF-HAp$_{U6}$.

2.7.2 Experimental design

The MOF-HAp nanocomposites were produced with varying factors, including the duration of biomimetic time and irradiation to ultrasound. MOF-HAp$_{U3}$ and MOF-HAp$_{U6}$ refer to samples synthesized with ultrasound irradiation at 3- and 6-h biomimetic time, while MOF-HAp$_{N3}$ and MOF-HAp$_{N6}$ are samples synthesized without ultrasound at the same varying biomimetic times.

The sampling method for the photocatalytic degradation of MET was developed at varying catalyst loading of MOF-HAp nanocomposite, initial concentrations of pollutant, and exposure time. The amount of photocatalyst was 0.25 and 0.5 g. The initial concentration of the pollutant has two levels: 8 and 12 ppm. It has undergone photocatalytic degradation at different exposure times: 0, 30, 60, 90, and 120 min. All samples were obtained in triplicate. In addition, MOF and HAp were prepared and underwent photocatalysis as control variables.

3 Results and Discussion

It was observed in Figure 2 that the samples were brownish-orange in color which was close to MOF's color, specifically the MIL-100 (Fe). This showed that the nanocomposite was mainly composed of MOF as compared to Hap, which was further explained in the characterizations done for the nanocomposites. Moreover, it coincides with the color of the MOFs synthesized in various literatures [9], [16].

3.1 *Characterization*

3.1.1 X-Ray Fluorescence (XRF)

In determining the elemental compositions present in the nanocomposite MOF-HAp, X-ray Fluorescence (XRF) analysis was performed. There is an evident detection of iron (Fe) and calcium (Ca), which are vital elements present in MOF and Hap, respectively. It was observed that the significant elements correlate with the elements determined in various related works [17], [18]. MOF-HAp assisted with ultrasound displayed better results as compared to MOF-HAp without the assistance of ultrasound. As seen in Table 1, MOF-HAp$_{U6}$ displayed the most dominant amount of iron and calcium as compared to the others. Moreover, the iron in MOF-HAp$_{N6}$ displayed the lowest amount of intensity. The dominance projected by MOF-HAp$_{U6}$ can be explained by ultrasound irradiation being an efficient technique for dispersing and deagglomerating particles, which leads to improved mixing and distribution of the elements [19]. Thus, potentially increasing the peaks indicated in the elemental analysis of MOF-HAp$_{U6}$.

Table 1: Elemental compositions based on XRF results

Elements	MOF-HApN3		MOF-HAp$_{N6}$		MOF-HApU3		MOF-HAp$_{U6}$	
	Conc. (%wt)	Intensity	Conc. (%wt)	Intensity	Conc. (%wt)	Intensity	Conc. (%wt)	Intensity
Fe	33.40	114304.43	38.88	14263.07	97.44	148327.26	55.93	2820597.56
Ca	1.45	377.56	1.49	463.83	2.19	506.75	1.57	12783.76
Al	65.08	41.88	59.56	40.05	0	0	42.27	677.49
Cl	0	0	0	0	0	0	0.23	257.60
Mo	0.07	436.25	0.07	452.90	0.36	485.51	0	0
Br	0	19.69	0	29.13	0.01	30.51	0	0
Cu	0	3.01	0	0	0.01	4.88	0	0
Zn	0	7.11	0	6.71	0	0	0	0

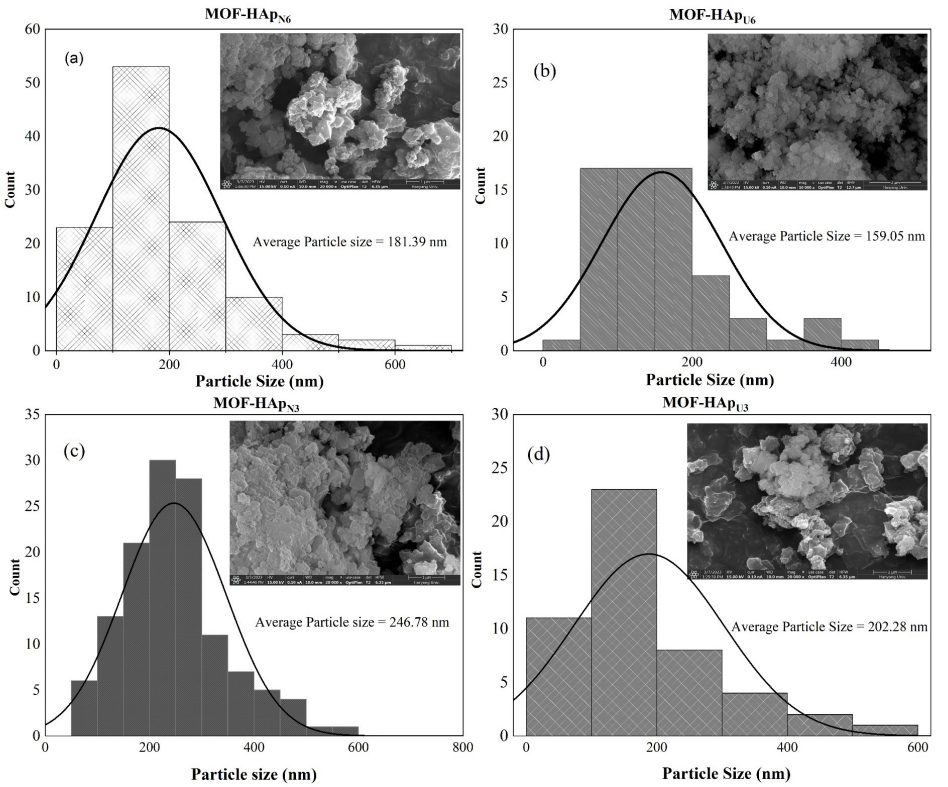

Figure 3: SEM results of the synthesized MOF-HAp nanocomposites: (a) MOF-HApN3, (b) MOF-HAp$_{N6}$, (c) MOF-HAp$_{U3}$, and (d) MOF-HAp$_{U6}$.

3.1.2 Scanning Electron Microscope (SEM)

The morphology and microstructure of the synthesized MOF-HAp were determined by SEM analysis, as shown in Figure 3. It can be observed that the synthesized MOF-HAp formed agglomerated particles owing to its non-uniform shape and size. The octahedral particles with distinct edges could be identified as MOF particles [17]. The smaller particles are expected to be HAp. HAp has no specific morphology, and the particles cluster to produce micron-sized spherical nanoaggregates with varying sizes of bone HAp crystals (length ranging from 30–50 nm, the width can be 15–30 nm, and thickness around 2–10 nm) [14]. With the longer biomimetic time and ultrasonic treatment, the nanocomposites were observed to have a more refined and consistent morphology. The morphology of the studied nanoparticles at shorter sonication times varied more in size and more clumping in their structures [20].

The size distribution of the nanocomposites under different biomimetic times, with and without the ultrasonic treatment, was measured using ImageJ software. The statistical results are shown in Figure 3. The synthesized MOF-HAp$_{N3}$ has an average particle size of 246.78 nm while MOF-HAp$_{N6}$ has an average particle size of 181.39 nm. For the ultrasound-assisted trials, MOF-HAp$_{U3}$ has an average particle size of 202.28 nm while MOF-HAp$_{U6}$ has an average particle size of 159.05 nm. Evidently, the longer the biomimetic time, the smaller the average particle size that can be produced which can be further reduced with ultrasonic treatment during the synthesis of the nanocomposites. With longer durations of sonication, noticeable crystals form, and their size decreases when subjected to continuous sonication. Having a smaller particle size was generally ideal as it indicated more surface area for the reaction, which ultimately means higher reactivity. In this study, the biomimetic time of 6 h with ultrasonic treatment produced the smallest average particle size [20], [21].

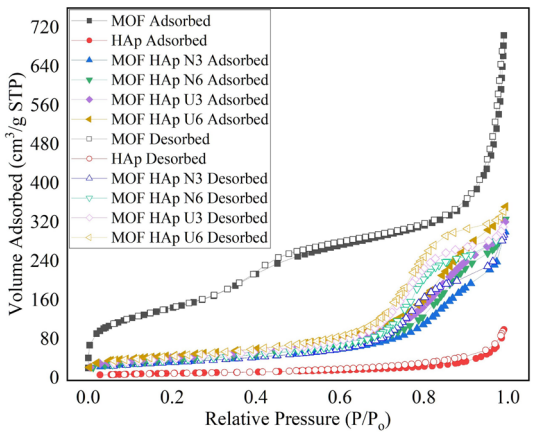

Figure 4: N_2 Adsorption/Desorption Isotherm Analysis.

3.1.3 Brunauer-Emmett-Teller (BET)

The textural properties, such as surface area, pore volume, and pore diameter, of the MOF-HAp samples were determined by N_2 adsorption/desorption isotherms (Figure 4) via Brunauer-Emmett-Teller (BET) analysis. The summary of results from the BET analysis can be seen in Table 2. MOF had the lowest pore diameter and the highest surface area and pore volume. On the other hand, the textural properties of HAp were completely reversed. Upon adding HAp via biomimetic synthesis, a significant reduction in surface area and pore volume was observed from the resulting nanocomposite. The decrease in porosity of the MOF-HAp proves the successful integration in the pores of MOF as HAp occupies areas within the nanocomposite [22], [23].

Table 2: Textural properties of MOF, HAp, and MOF-HAp samples

Material	Surface Area (m^2/g)	Pore Volume (cm^3/g)	Pore Diameter (nm)
MOF	1051.20	0.90	6.95
HAp	35.98	0.15	17.66
MOF-HAp_{N3}	114.45	0.44	16.67
MOF-HAp_{N6}	130.91	0.47	14.81
MOF-HAp_{U3}	147.53	0.49	13.09
MOF-HAp_{U6}	163.95	0.54	13.04

Among the MOF-HAp samples, the surface area of the synthesized MOF-HAp with ultrasound was higher than those synthesized without ultrasound. The high surface area of the catalyst stimulates the dispersion of small-sized nanomaterials which means that a larger interaction area is available for the elimination of the pollutant [23]. A similar trend was observed for the pore volume of the MOF-HAp samples. For the pore diameter, MOF-HAp samples synthesized with ultrasound had a lower pore volume than those synthesized without ultrasound.

3.1.4 X-Ray Diffraction (XRD)

The phase purity and crystallinity of the MOF-HAp nanocomposites were examined using X-ray Diffraction (XRD). As shown in Figure 5, the peaks of MOF-HAp with ultrasound and without ultrasound in 3 and 6 h matched well with the peaks of standard MOF. All MOF-HAp samples demonstrated a sharp peak at $2\theta = 20$, 24, and 28°similar to the standard MOF. The clear and sharp peaks showed good crystallinity of the catalyst. The experimental XRD pattern contains identical relative intensities of each predicted peak from the XRD pattern that was simulated using the MIL-100 (Fe) cif file. In addition, the 2θ positions of these XRD peaks matched very well with any accumulation of the narrow peaks of the pattern of the sample MIL-100 (Fe) [9]. The peaks of HAp were smooth and clear low-angle peaks. The HAp was observed on the peaks of the MOF-HAp samples as shown in Figure 5, where it exhibited an amorphous peak at $2\theta = 32$ and 33°. The spectra showed characteristic peaks of HAp ($2\theta = 32$ and 33°). The amorphous HAp structure is shown by the spectra having more broad peaks than the crystalline HAp structure. The biological apatite pattern is comparable to this crystallographic behavior [14].

The peaks of nanocomposites under different biomimetic times, with and without the ultrasonic treatment were determined by XRD. The synthesized MOF-HAp_{N3}, MOF-HAp_{N6}, MOF-HAp_{U3} and MOF-HAp_{U6} exhibited a peak at $2\theta = 20$, 24, 28, 32, 39, 42, 44 and 61° shown in Figure 5. Compared to the MOF, all the MOF-HAp nanocomposites had a less crystalline nature due to the addition of the amorphous HAp [22]. The peaks of MOF-HAp with and without ultrasound have almost similar sharpness in their peaks. However, the peaks of MOF-HAp_{U3} and MOF-HAp_{U6} have a slightly broader base than MOF-HAp_{N3} and MOF-HAp_{N6}. The broader base of

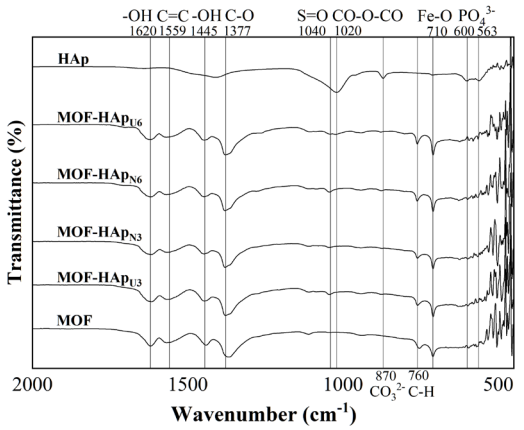

Figure 6: FTIR spectral interpretation.

the peaks indicated an amorphous nature but as it is in combination with the sharp peaks, the MOF-HAp nanocomposites can be determined to have a semicrystalline nature. The exposure to ultrasonic irradiation after a few minutes reduces crystallinity [21]. HAp had smooth and clear low-angle peaks.

3.1.5 Fourier Transform Infrared (FTIR)

The wavelength of interest for the interpretation of FTIR transmittance spectra (Figure 6) for synthesized MOF, HAp, and MOF-HAp are identified to show proof of the presence or absence of significant functional groups and to determine the synthesis of the nanocomposite.

Table 3 shows a summary of the FTIR spectral interpretation wherein the results of the IR reading of the MOF exhibited clear adsorption at 1620, 1559, 1445, 1377, 760, and 710 cm^{-1}. The peak at 1620 cm^{-1} is assigned to bonds of carboxylate groups, while the bands at 1442 and 1371 cm^{-1} are respectively attributed to asymmetric and symmetric vibrational bands characteristic of the -O-C-O- group. The other two sharp peaks at 760 and 707 cm^{-1} correspond to C–H bending vibrations of benzene which were consistent with the findings of other related articles [16], [22]. The presence of benzene is attributed to the unreacted trimesic acid during the synthesis of the MOF. It is concluded from the Fe-O peak at 712 cm^{-1}, to ascertain that the unreacted Trimesic acid species have been effectively removed in their purification step and these molecules were coordinated with the iron atoms of the MOF framework [24]. The excess in the nanocomposite may be attributed to unreacted $FeCl_2$ and trimesic acid during the synthesis of the MOF.

As for the HAp, the absorption bands at ~562, 601, 954, and 1020 cm^{-1} detected in the spectra of precipitated HA samples were attributed to the phosphate (PO_4^{3-}) ion, and at around 1470–1410 cm^{-1} and 870 cm^{-1} suggest the presence of carbonate (CO_3^{2-}) [14]. The FTIR results clearly point to the substitution of the CO_2^{3-} into the apatite by ultrasonic heating that resulted in the formation of carbonated HA, similar to the microwave heating results [14].

Generally, the nanocomposites subjected to

Table 3: FTIR spectral interpretation

Significant wavenumber (cm^{-1})	Interpretation	MOF	MOF-HAp$_{N3}$	MOF-HAp$_{N6}$	MOF-HAp$_{U3}$	MOF-HAp$_{U6}$	HAp
3200–3400	-OH stretching	Broad Medium	Broad Medium	Broad Weak	Broad Medium	Broad Weak	Broad Weak
1620	C=O stretching	Narrow Medium	Medium	Medium	Medium	Medium	Absent
1559	C=C stretching	Broad Medium	Broad Medium	Broad Medium	Broad Medium	Broad Medium	Absent
1445	-OH vibration	Narrow Medium	Narrow Medium	Narrow Medium	Narrow Medium	Narrow Medium	Absent
1377	C-O vibration	Narrow Strong	Broad Strong	Broad Strong	Broad Strong	Broad Strong	Absent
1040	S=O stretching	Weak	Narrow Weak	Narrow Weak	Narrow Medium	Wide Medium	Overlap, Wide Strong
1020	CO-O-CO stretching	Absent	Absent	Absent	Absent	Medium	Overlap, Wide Strong
940	C-H bending	Weak	Weak	Weak	Weak	Weak	Absent
876	-	Absent	Weak	Weak	Weak	Weak	Medium
760	C–H bending vibrations of benzene	Medium	Narrow Medium	Narrow Medium	Narrow Medium	Narrow Medium	Absent
710	-	Narrow Medium	Narrow Medium	Narrow Medium	Narrow Medium	Narrow Medium	Weak

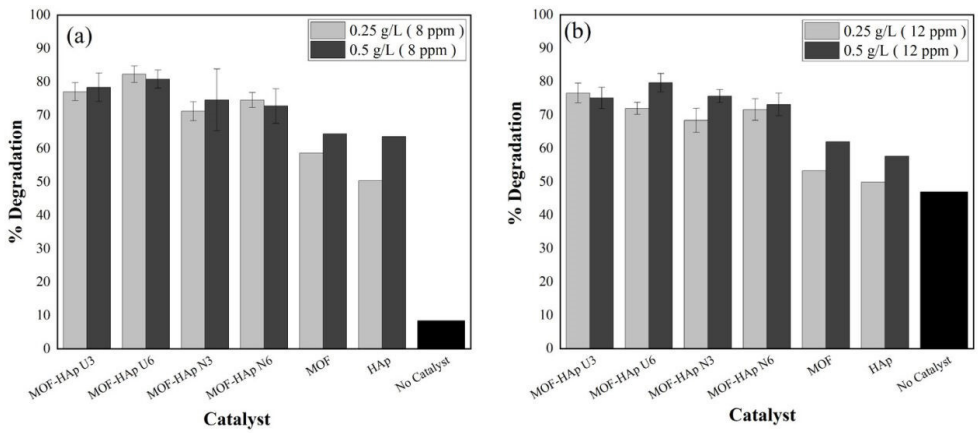

Figure 7: Percent degradation of MET concentration at different catalyst loading for 120 min exposure time, (a) 8 ppm and (b) 12 ppm.

ultrasound displayed lower transmissions at 1620, 1559, 1445, 1377, 760, and 710 cm^{-1} compared to the ones without ultrasound, making them more similar to the original MOF. Signifying the effect of the additional energy provided by the ultrasound leading to the creation of more bonds in these wavelengths. Ultrasonication during the synthesis causes a curious agglomeration, presumably due both to an ultrasonic-induced collision and to surface activity [22].

Furthermore, the fingerprint region of all the varying synthesized nanocomposites was also consistent with the fingerprint region of both the control MOF and control HAp although the peaks have slightly shifted. There were also no stray reagents present in the FTIR analysis.

3.2 *Photocatalytic degradation*

At the 8 ppm initial pollutant concentration, the absence of the catalyst resulted in minimal degradation. Comparing no catalyst and the control MOF and HAp, it can be seen that the control MOF and HAp, have a noticeable reduction. Figure 7(a) shows that with a catalyst loading of 0.25 g/L, MOF-HAp_{U3} has a percent degradation of 77.04%. MOF-HAp_{U6} has an average percent degradation of 82.25%. The average percent degradation of MOF-HAp_{N3} is 79.20% and the MOF-HAp_{N6} is 74.51%. Moreover, the no catalyst has a percent degradation of 8.44 % and the control MOF and HAp have an average percent degradation of 58.65% and 50.36%, respectively. With 0.5 g/L of catalyst loading, MOF-HAp_{U3} has a percent degradation of 78.38 %. MOF-HAp_{U6} has an average percent degradation of 80.80%. The average percent degradation of MOF-HAp_{N3} is 74.58% and the MOF-HAp_{N6} is 72.75%. The control MOF has an average percent degradation of 64.38% and HAp has an average percent degradation of 63.61%. Individually, the control MOF and HAp are effective in the degradation of MET. However, for both catalyst loadings, MOF-HAp_{U6} was found to have the highest average percent degradation.

In the absence of the catalyst, the degradation percentage was noticeable at the 12 ppm initial concentration. The average percent degradation for 12 ppm initial concentration with varying catalyst loading is depicted in Figure 7(b). With 0.25 g/L catalyst loading, the average percentage values were 76.55%, 71.93%, 71.61%, and 68.38%, for MOF-HAp_{U3}, MOF-HAp_{U6}, MOF-HAp_{N6} and MOF-HAp_{N3}, respectively. Moreover, the no catalyst has an average percent degradation of 46.96 % and the control MOF has an average percent degradation of 53.27% and HAp has a value of 49.87%. The catalyst with the highest average percent degradation is MOF-HAp_{U3}. Although it was observed that MOF-HAp_{U3} has the highest average percent degradation, MOF-HAp_{U6} has a more precise set of data showing a more consistent degradation. The standard deviation of MOF-HAp_{U6} is 1.81, in contrast to MOF-HAp_{U3} with 2.97.

On the other hand, the average percent degradation of MET with 0.5 g/L catalyst loading resulted in

relatively low values of 75.08%, 79.66%, 75.63%, and 73.17% for MOF-HAp_{U3}, MOF-HAp_{U6}, MOF-HAp_{N6}, and MOF-HAp_{N3}, respectively. The control MOF and HAp have an average percent degradation of 61.98% and 57.62%, respectively. The catalyst with the highest average percent degradation is MOF-HAp_{U6}.

No catalyst in the degradation of MET showed a minimal degradation percentage. With higher concentrations, it showed a greater percentage of degradation. Moreover, the MOF and HAp catalysts showed a greater degradation percentage compared to no catalyst since the use of catalysts increased the photocatalytic activity [25].

The percent degradation of MOF-HAp nanocomposite was seen to have greater efficiency than that of the control catalysts, MOF and HAp. Synthesized MOF-HAp with the assistance of ultrasound is found to further increase the percent degradation of MET, particularly MOF-HAp_{U6}. Considering the high intensity of Fe found in the ultrasound-assisted MOF-HAp, the presence of this inorganic compound catalyzes the photo Fenton reaction, which accelerates the photocatalytic degradation [6], [26]. The photo-Fenton reaction enhanced the generation of hydroxyl radicals which improved the efficiency and speed of the degradation process, making it more effective for the removal of MET. Moreover, MOF-HAp's effective ability in photocatalytic degradation is attributed to its small particles, high surface area, high pore volume, and low pore diameter. Concurring with various findings, increased pore volume, porosity, and surface area significantly enhance the catalytic effectiveness of a catalyst, particularly in the presence of environmental pollutants. A catalyst with a greater pore volume provides more room for reactant molecules to engage with the catalyst, while heightened porosity offers more openings for reactants to reach. Moreover, an expanded surface area offers more active regions where pollutants can bind and partake in chemical reactions. These attributes play a crucial role by facilitating the interaction and attachment of pollutants to the catalyst's active sites. [27]–[29]. Although MOF-HAp synthesized without ultrasound is found to have better crystallinity, crystalline size has a more significant effect on photoreactivity than crystallinity [30]. The findings of their research emphasized that crystallinity had a negligible effect on photodecomposition, which contradicts various studies [31], [32].

Comparing the catalyst loading, it was observed that the lower catalyst loading concentration has greater efficiency. At lower MET concentrations, increasing the catalyst dosage reduced degradation efficiency. However, increasing the catalyst dosage considerably enhanced MET degradation efficiency at higher MET concentrations [33].

Various methods were investigated for photodegrading MET in water under UV radiation, comparing the effectiveness of different catalysts such as photolysis, TiO_2, 5% ZrO_2–TiO_2, 5% TiO_2–ZrO_2 and ZrO_2. The study observed that the degradation of MET ranged from 28–52% when using different treatment processes with an initial MET concentration of 10 mg/L and a catalyst loading of 0.5 g/L [2]. With the same parameters, exposure to MOF-HAp led to MET degradation ranging from 72% to 81%. This underscores the potential of the MOF-HAp nanocomposite as a more effective choice compared to chemically produced TiO_2, a commonly used substance in treating water and wastewater.

3.3 *Effects of Parameters to the Photocatalytic Degradation of MET*

3.3.1 Initial pollutant concentration

Without the use of the catalyst, it was noticed that the decrease in the concentration of the 8 ppm pollutant was almost negligible, as can be seen in Figures 8(a) and (b). On the other hand, the degradation of the 12 ppm pollutant concentration in Figures 8(c) and (d) without any catalyst had a significant decrease compared to the degradation of 8 ppm concentration. Once the light reaches the surface of the pollutant, photoabsorption will happen, which will transform MET into an active MET allowing direct photolysis to occur. 12 ppm initial concentration allowed more light to interact with its particles that performed photoabsorption on its surface which led to its photolysis [34].

Comparing Figures 8(b) and (d) where photocatalysts were used, it can be seen that Figure 8(b) has the lower final concentrations of pollutant at different types of photocatalysts because of its lower initial concentration of pollutant which was 8 ppm. At 120 min of photocatalytic degradation in Figure 8(b), MOF-HAp_{U6} had the lowest final concentration of the pollutant

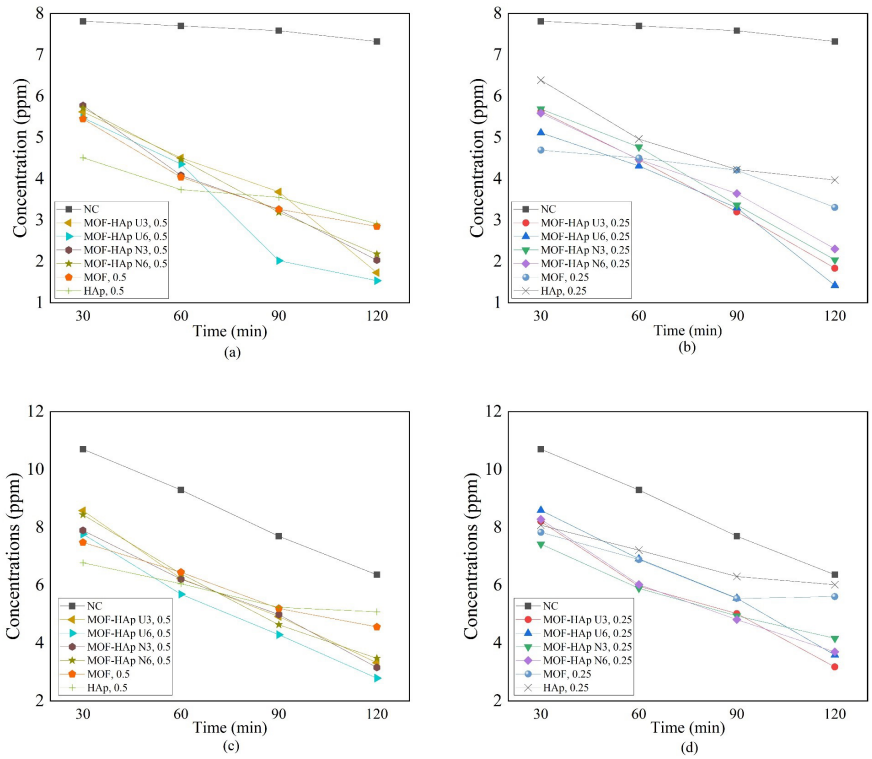

Figure 8: Concentration vs time at varying initial concentration and catalyst loading: (a) 8 ppm, 0.5 g/L, (b) 8 ppm, 0.25 g/L, (c) 12 ppm, 0.5 g/L, and (d) 12 ppm, 0.25 g/L.

that reached 86% degradation. Figure 8(d) which had a 12 ppm initial concentration of pollutant showed the lowest final concentration of MET at 120 min of degradation when MOF-HAp$_{U3}$ was used. This was the most efficient catalyst to be used for 12 ppm of pollutant concentration having reached a percent degradation of 83%.

The percent degradation was higher at a lower initial pollutant concentration of 8 ppm than the 12 ppm. The light at 8 ppm initial pollutant concentration reached more of the surface of the photocatalyst which helped the photocatalyst and pollutant particle to have more interaction that resulted in effective photocatalytic degradation of MET. While the 12 ppm concentration had more particles that hindered the light from reaching the surface of the photocatalyst, which proceeded to less degradation of the pollutant [35].

Both Figures 8(a) and (c) contained 0.5 g/L of catalyst loading but Figure 8a has a lower initial concentration of pollutants that resulted in a higher percent of degradation. 8 ppm produced a lower final concentration because light was able to pass through the solution of catalyst and pollutant that activated its photocatalysis. Moreover, the higher concentration of catalyst loading helped in the degradation of the low initial concentration of pollutant because more active sites were present [35]. Whereas the 12 ppm initial concentration together with higher catalyst loading was more turbid so light was hindered by a great number of particles that prevented it from reaching the surface of the catalyst [36].

3.3.2 Catalyst loading

Varying catalyst loading was used in each initial concentration of pollutant. Figures 8(a) and (b) showed 0.5 and 0.25 g/L of catalyst loading for an 8 ppm concentration of the pollutant. It can be observed that Figure 8(a) has a more clustered final concentration while Figure 8(b) has a scattered orientation of final concentration. The controls, which were the MOF and HAp in Figure 8(a), produced a lower final concentration

at the 120 min mark compared to the ones in Figure 8(b). This showed that a higher catalyst loading gave a higher degradation, at least for the controls. When it comes to MOF-HAp catalysts, the lowest final concentration in Figure 8(b) at 120 min is comparatively lower than in Figure 8(a). The most efficient catalyst that was used in Figure 8(b) was MOF-HAp$_{U6}$, which was the same catalyst that had the lowest final concentration in Figure 8(a) but at a different catalyst loading. It meant that the lower catalyst loading provided more paths for light to pass through and come into contact with the surface of the photocatalysts, which yielded higher degradation [36].

Figures 8(c) and (d) showed the effect of catalyst loading on the initial pollutant concentration of 12 ppm. Comparing the two figures, we infer that Figure 8(c) has a lower final concentration for the controls, which were MOF and HAp for 120 min. This meant that higher catalyst loading for controls resulted in a higher percentage of degradation. The same result happened in MOF-HAp catalysts where the final concentration of the pollutant was lowest when the catalyst loading was higher. MOF-HAp$_{U6}$ was the best catalyst in Figure 8(c) while MOF-HAp$_{U3}$ was the best in Figure 8(d). Overall, catalyst loading of 0.5 g/L provided the highest degradation due to the great number of active sites present with the catalysts that the light came into contact with. Lower catalyst loading provided a smaller number of active sites where degradation could happen which translated to a lower percentage of degradation [36].

From the results, it was found that as the concentration of the photocatalyst increased, the degradation increased as well, but only to a limited amount of photocatalyst due to the blocking of the path of light when too many photocatalyst molecules were present. A greater number of molecules of the photocatalyst resulted in higher turbidity, which led to lesser interaction between pollutant and photocatalyst particles because the light was not able to strike the surface of the molecule of the photocatalyst [36].

3.3.3 Exposure time

MOF and HAp, both at 0.5 g/L, in Figure 8(a) showed a decrease in pollutant concentration as time increased. HAp had a lower decrease in pollutant concentration as compared to MOF at 30 min, but at 120 min, MOF had a lower final pollutant concentration when compared to HAp. Out of all the photocatalysts that were used, MOF-HAp$_{U6}$ at 0.5 g/L concentration had the lowest final pollutant concentration, so it was the most efficient for photocatalytic degradation of MET in Figure 8(a). It started slowly for the first 60 min of degradation time but a sudden drop in pollutant concentration happened at the 90 min mark and continued to decrease until 120 min of degradation time.

In Figure 8(b), MOF at 0.25 g/L concentration showed a significant decrease at 30 min compared to the pollutant concentration without any catalyst added and the other photocatalyst that was used. Over time, it showed a minute decrease in the concentration of the pollutant up until the 120 min mark so it can be translated to a low efficiency of degradation. On the other hand, HAp could also be considered to have the same efficiency of degradation due to the slight difference in concentration of the pollutant starting from the 60–120 min mark. Comparing all the photocatalysts that were used in Figure 8(b), it was determined that MOF-HAp$_{U6}$ had the lowest final concentration of pollutant after 120 min of degradation. Moreover, MOF-HAp photocatalysts were able to yield lower final concentrations in comparison to MOF and HAp which were the controls of the experiment.

Garnering the data for Figure 8(a) and (b), the pollutant degradation at 30 min is between 23–39%; at 60 min, degradation is between 39–53%; at 90 min, 53–74% and at 120 min, 74–86%. The graphs in Figure 8(c) and (d) showed that the final concentration of photolysis was not on par with the final concentration of photocatalytic degradation. The photolysis of the 12 ppm pollutant concentration was due to the photoabsorption that happened on its surface because light was able to interact with its great number of particles [34]. As the number of particles increases, more interactions will occur that will result in a higher percentage of degradation.

The MOF and HAp controls in Figure 8(c) have lower pollutant concentrations at 30 min of degradation time compared to the MOF-HAp photocatalysts. But when it reached the 120 min mark, the opposite happened where MOF-HAp photocatalysts had the lower pollutant concentrations compared to MOF and HAp. The MOF-HAp photocatalysts had the same decreasing trend in the graph and were at almost the same level of degradation at every time interval.

However, the one that had the lowest final pollutant concentration was the MOF-HAp_{U6}, which indicated that it has the highest efficiency when it comes to photocatalytic degradation of MET.

Figure 8(d) showed the pollutant concentration at the 120 min mark was noticeably higher than its 90 min concentration when MOF was used while the HAp had a decreasing trend shown in the graph. MOF might not be attributed to an error in the preparation of the sample or a malfunction of the equipment used because the concentration of the pollutant had a noticeable increase. Between 60 and 90 min, the remaining pollutant concentrations of MOF-HAp_{U3}, MOF-HAp_{N3}, and MOF-HAp_{N6} were almost the same while MOF and MOF-HAp_{U6} had similar levels of degradation for the same time interval. In this graph, MOF-HAp_{U3} had the lowest concentration when 120 min of degradation time was reached so it has the most efficient degradation capability out of all the photocatalysts that were used in the degradation of 12 ppm pollutant concentration.

Generally, the pollutant degradation data for Figure 8(c) and (d) are the following: at 30 min, degradation was between 22–39%; at 60 min, degradation was between 39–52%; at 90min, 52–64% and at 120 min, 64–85%

Figure 8 shows the relationship between concentration and time with the given catalyst loading. The concentration of the pollutant, MET, decreased in concentration as time passed because high concentration was degraded through photocatalytic degradation. Longer time meant that the pollutant and photocatalyst particles had longer interaction with one another, which resulted in lower final concentration of the pollutant. Regardless of the initial concentration of the pollutant, the final concentration lowered as time progressed in both photolysis and photocatalyst degradation [36]. The final concentration of the pollutant varied depending on its initial concentration and the catalyst loading.

4 Conclusions

In this study, the MOF-HAp nanocomposite was successfully produced using a 10xSBF-like solution via ultrasound-assisted biomimetic synthesis and was proven to be an effective photocatalyst in the degradation of MET.

To confirm the physicochemical properties of the produced MOF-HAp, various characterizations were done. Findings of the XRF analysis indicated that the intensities and concentrations of iron and calcium, essential elements of MOF and HAp, were higher in MOF-HAp nanocomposites synthesized with ultrasound compared to the synthesized nanocomposites without ultrasound, particularly MOF-HAp_{U6}. Based on the SEM analysis, MOF-HAp_{U6} produced the smallest average particle size which implied high surface area for reactivity. MOF-HAp_{U6} was confirmed to have a higher surface area and pore volume than MOF-HAp samples synthesized without ultrasound and lower biomimetic times. MOF-HAp had a lower surface area and pore volume than that of pristine MOF due to the addition of the HAp. MOF-HAp_{U3} and MOF-HAp_{U6} were found to possess a semicrystalline nature, as shown by the XRD analysis. Furthermore, as seen in the FTIR analysis, the nanocomposites subjected to ultrasound exhibited lower transmissions at certain wavelengths compared to the produced MOF-HAp without ultrasound.

The synthesized MOF-HAp's potential as a photocatalyst for degrading MET was investigated in this study. MOF-HAp, in general, was able to reduce the initial pollutant concentration with greater effectiveness in comparison to having only MOF or HAp as the photocatalysts. It is also worth noting that samples of the MOF-HAp nanocomposites that were synthesized with the assistance of ultrasound showed better photocatalytic degradation capabilities than the MOF-HAp samples synthesized without ultrasound. Furthermore, between MOF-HAp_{U3} and MOF-HAp_{U6}, results show that the latter is a better photocatalyst than the former. Therefore, among the four types of MOF-HAp nanocomposites that were used in the photocatalytic degradation of MET, MOF-HAp_{U6} demonstrated the best results by having the highest average percent reduction.

The photocatalytic degradation effects of initial concentration, catalyst loading, and exposure time were also evaluated. The highest degrading efficiency of MET was attained at a specific set of parameters: 8 ppm of initial pollutant concentration, 0.25g of catalyst loading, and 120 min of exposure time. Results showed that with a lower initial pollutant concentration of 8 ppm, the degradation efficiency was higher. Additionally, the 0.25 g/L of catalyst loading was able

to degrade a higher pollutant concentration than the higher catalyst loading of 0.5g/L. It was also visible that the relationship between concentration and time was inversely proportional wherein as time increased, the concentration decreased. Hence, 120 min of exposure time was able to degrade more of the pollutant.

Acknowledgments

The researchers express their sincere gratitude to the Chemical Engineering Laboratory headed by Engr. Albert Evangelista and Adamson Chemistry Laboratory headed by Ms. Cindy Bautista for their assistance in our laboratory needs. Their help is irreplaceable, and their generosity to the researchers is unparalleled.

Author Contributions

M.E.: conceptualization, investigation, methodology, data curation, data analysis; E.G.: conceptualization, investigation, data curation, data analysis; L.M.: conceptualization, investigation, methodology, data curation, data analysis; C.S.: conceptualization, investigation, methodology, data analysis, reviewing and editing; J.S.: conceptualization, investigation, data curation, data analysis; N.S.: conceptualization, investigation, data analysis; R.V.R: conceptualization, research design, reviewing and project administration.; R.R.: investigation and reviewing. All authors have read and agreed to the published version of the manuscript.

Conflicts of Interest

The authors declare no conflict of interest.

References

[1] S. Foteinis and E. Chatzisymeon, "Heterogeneous photocatalysis for water purification," in *Nanostructured Photocatalysts*. Amsterdam, Netherlands: Elsevier, pp. 75–97, 2020, doi: 10.1016/b978-0-12-817836-2.00004-1.

[2] C. F. Carbuloni, J. E. Savoia, J. S. Santos, C. A. Pereira, R. G. Marques, V. A. Ribeiro, and A. M. Ferrari, "Degradation of metformin in water by TiO_2–ZrO_2 photocatalysis," *Journal of Environmental Management*, vol. 262, 2020, Art. no. 110347, doi: 10.1016/j.jenvman.2020.110347.

[3] G. A. Elizalde-Velázquez and L. M. Gómez-Oliván, "Occurrence, toxic effects and removal of metformin in the aquatic environments in the world: Recent trends and perspectives," *Science of The Total Environment*, vol. 702, 2020, 134924, doi: 10.1016/j.scitotenv.2019.134924.

[4] P. Venkatesan, P. Kumari, and N. Remya, "Solar photocatalytic degradation of metformin by TiO_2 synthesized using Calotropis gigantea leaf extract," *Water Science and Technology*, vol. 83, no. 5, pp. 1072–1084, 2021, doi: 10.2166/wst.2021.040.

[5] W. S. Koe, J. W. Lee, W. C. Chong, Y. L. Pang, and L. C. Sim, "An overview of photocatalytic degradation: photocatalysts, mechanisms, and development of photocatalytic membrane," *Environmental Science and Pollution Research*, vol. 27, no. 3, pp. 2522–2565, 2019, doi: 10.1007/s11356-019-07193-5.

[6] R. V. C. Rubi, J. G. Olay, P. B. G. Caleon, R. A. F. De Jesus, M. B. L. Indab, R. C. H. Jacinto, M. S. Sabalones, F. dela Rosa, and N. L. Hamidah, "Photocatalytic degradation of diazinon in g-C3N4/Fe(III)/persulfate system under visible LED light irradiation," *Applied Science and Engineering Progress*, vol. 14, no. 1, pp. 100–107, 2021, doi: 10.14416/j.asep.2020.12.008.

[7] H. Kumari, Sonia, Suman, R. Ranga, S. Chahal, S. Devi, S. Sharma, S. Kumar, P. Kumar, S. Kumar, A. Kumar, and R. Parmar, "A review on photocatalysis used for wastewater treatment: Dye degradation," *Water Air and Soil Pollution*, vol. 234, no. 6, May 2023, Art. no. 349, doi: 10.1007/s11270-023-06359-9.

[8] M. P. Reddy, A. Venugopal, and M. Subrahmanyam, "Hydroxyapatite photocatalytic degradation of calmagite (an azo dye) in aqueous suspension," *Applied Catalysis B-environmental*, vol. 69, no. 3–4, pp. 164–170, Jan. 2007, doi: 10.1016/j.apcatb.2006.07.003.

[9] K. Guesh, C. A. D. Caiuby, A. Mayoral, M. Díaz-García, I. Díaz, and M. Sánchez-Sánchez, "Sustainable preparation of MIL-100(FE) and its photocatalytic behavior in the degradation of methyl orange in water," *Crystal Growth & Design*, vol. 17, no. 4, pp. 1806–1813, Mar. 2017, doi: 10.1021/acs.cgd.6b01776.

[10] M. Samy, M. G. Ibrahim, M. Fujii, K. E. Diab,

M. F. Elkady, and M. G. Alalm, "CNTs/MOF-808 painted plates for extended treatment of pharmaceutical and agrochemical wastewaters in a novel photocatalytic reactor," *Chemical Engineering Journal*, vol. 406, Feb. 2021, Art. no. 127152, doi: 10.1016/j.cej.2020.127152.

[11] M. Dubey, N. V. Challagulla, S. Wadhwa, and R. Kumar, "Ultrasound assisted synthesis of magnetic Fe_3O_4/α-MnO_2 nanocomposite for photodegradation of organic dye," *Colloids and Surfaces A: Physicochemical and Engineering Aspects*, vol. 609, Jan. 2021, Art. no. 125720, doi: 10.1016/j.colsurfa.2020.125720.

[12] A. R. Abbasi, M. Karimi, and K. Daasbjerg, "Efficient removal of crystal violet and methylene blue from wastewater by ultrasound nanoparticles Cu-MOF in comparison with mechanosynthesis method," *Ultrasonics Sonochemistry*, vol. 37, pp. 182–191, Jul. 2017, doi: 10.1016/j.ultsonch.2017.01.007.

[13] T. Xia, Y. Lin, W. Li, and J. Mei, "Photocatalytic degradation of organic pollutants by MOFs based materials: A review," *Chinese Chemical Letters*, vol. 32, no. 10, pp. 2975–2984, Oct. 2021, doi: 10.1016/j.cclet.2021.02.058.

[14] T. T. Demirtaş, G. Kaynak, and M. Gümüşderelioğlu, "Bone-like hydroxyapatite precipitated from 10×SBF-like solution by microwave irradiation," *Materials Science and Engineering*: C, vol. 49, pp. 713–719, Apr. 2015, doi: 10.1016/j.msec.2015.01.057.

[15] E. Aseman-Bashiz and H. Sayyaf, "Metformin degradation in aqueous solutions by electro-activation of persulfate and hydrogen peroxide using natural and synthetic ferrous ion sources," *Journal of Molecular Liquids*, vol. 300, Feb. 2020, Art. no. 112285, doi: 10.1016/j.molliq.2019.112285.

[16] B. Souza, A. F. Möslein, K. Titov, J. D. Taylor, S. Rudić, and J.-C. Tan, "Green reconstruction of MIL-100 (FE) in water for high crystallinity and enhanced guest encapsulation," *ACS Sustainable Chemistry & Engineering*, vol. 8, no. 22, pp. 8247–8255, May 2020, doi: 10.1021/acssuschemeng.0c01471.

[17] R. Nivetha, K. Gothandapani, V. Raghavan, G. Jacob, R. Sellappan, P. Bhardwaj, S. Pitchaimuthu, A. N. M. Kannan, S. K. Jeong, and A. N. Grace, "Highly porous MIL-100(FE) for the hydrogen evolution reaction (HER) in acidic and basic media," *ACS Omega*, vol. 5, no. 30, pp. 18941–18949, Jul. 2020, doi: 10.1021/acsomega.0c02171.

[18] S. Sebastiammal, A. S. L. Fathima, S. Devanesan, M. S. AlSalhi, J. Henry, M. Govindarajan, and B. Vaseeharan, "Curcumin-encased hydroxyapatite nanoparticles as novel biomaterials for antimicrobial, antioxidant and anticancer applications: A perspective of nano-based drug delivery," *Journal of Drug Delivery Science and Technology*, vol. 57, Jun. 2020, Art. no. 101752, doi: 10.1016/j.jddst.2020.101752.

[19] A. Sánchez-Hernández, J. Martínez-Juárez, J. J. Gervacio-Arciniega, R. Silva-González, and M. J. Robles-Águila, "Effect of ultrasound irradiation on the synthesis of Hydroxyapatite/Titanium oxide nanocomposites," *Crystals*, vol. 10, no. 11, p. 959, Oct. 2020, doi: 10.3390/cryst10110959.

[20] H. R. Mendoza, J. Jordens, M. V. L. Pereira, C. Lutz, and T. Van Gerven, "Effects of ultrasonic irradiation on crystallization kinetics, morphological and structural properties of zeolite FAU," *Ultrasonics Sonochemistry*, vol. 64, Jun. 2020, Art. no. 105010, doi: 10.1016/j.ultsonch.2020.105010.

[21] A. O. Lobo, H. Zanin, I. A. W. B. Siqueira, N. C. S. Leite, F. R. Marciano, and E. J. Corat, "Effect of ultrasound irradiation on the production of nHAp/MWCNT nanocomposites," *Materials Science and Engineering: C*, vol. 33, no. 7, pp. 4305–4312, Oct. 2013, doi: 10.1016/j.msec.2013.06.032.

[22] B. T. Le, D. D. La, and P. T. H. Nguyen, "Ultrasonic-Assisted fabrication of MIL-100(FE) Metal–Organic frameworks as a carrier for the controlled delivery of the chloroquine drug," *ACS Omega*, vol. 8, no. 1, pp. 1262–1270, Dec. 2022, doi: 10.1021/acsomega.2c06676.

[23] A. A. Aabid, J. I. Humadi, G. S. Ahmed, A. T. Jarullah, M. A. Ahmed, and W. S. Abdullah, "Enhancement of desulfurization process for light gas oil using new zinc oxide loaded over alumina nanocatalyst," *Applied Science and Engineering Progress*, vol. 16, no. 3, Feb. 2023, Art. no. 6756, doi: 10.14416/j.asep.2023.02.007.

[24] C. Jian-Hua, X. Wang, Y. Zhou, J. Li, and

C. Wang, "Selective adsorption of arsenate and the reversible structure transformation of the mesoporous metal–organic framework MIL-100(Fe)," *Physical Chemistry Chemical Physics*, vol. 18, no. 16, pp. 10864–10867, Jan. 2016, doi: 10.1039/c6cp00249h.

[25] M. B. Tahir, M. Sohaib, M. Sagir, and M. Rafique, "Role of nanotechnology in photocatalysis," in *Encyclopedia of Smart Materials*. Amsterdam, Netherlands: Elsevier, pp. 578–589, 2022, doi: 10.1016/b978-0-12-815732-9.00006-1.

[26] V.-H. Nguyen, S. M. Smith, K. Wantala, and P. Kajitvichyanukul, "Photocatalytic remediation of persistent organic pollutants (POPs): A review," *Arabian Journal of Chemistry*, vol. 13, no. 11, pp. 8309–8337, Nov. 2020, doi: 10.1016/j.arabjc.2020.04.028.

[27] S. Gahlot, F. Dappozze, S. Mishra, and C. Guillard, "High surface area g-C3N4 and g-C_3N_4-TiO_2 photocatalytic activity under UV and Visible light: Impact of individual component," *Journal of Environmental Chemical Engineering*, vol. 9, no. 4, Aug. 2021, Art. no. 105587, doi: 10.1016/j.jece.2021.105587.

[28] D. Li, H. Song, X. Meng, T. Shen, J. Sun, W. Han, and X. Wang, "Effects of particle size on the structure and photocatalytic performance by Alkali-Treated TIO_2," *Nanomaterials*, vol. 10, no. 3, p. 546, Mar. 2020, doi: 10.3390/nano10030546.

[29] S. Estrada-Flores, C. M. Pérez-Berumen, L. A. García-Cerda, and T. E. Flores-Guía, "Relationship between morphology, porosity, and the photocatalytic activity of TiO_2 obtained by sol–gel method assisted with ionic and nonionic surfactants," *Boletin De La Sociedad Espanola De Ceramica Y Vidrio*, vol. 59, no. 5, pp. 209–218, Sep. 2020, doi: 10.1016/j.bsecv.2019.10.003.

[30] A. B. D. Nandiyanto, R. Zaen, and R. Oktiani, "Correlation between crystallite size and photocatalytic performance of micrometer-sized monoclinic WO_3 particles," *Arabian Journal of Chemistry*, vol. 13, no. 1, pp. 1283–1296, Jan. 2020, doi: 10.1016/j.arabjc.2017.10.010.

[31] F. Yang, J. Qu, Y. Zheng, Y. Cai, X. Yang, C. M. Li, and J. Hu, "Recent advances in high-crystalline conjugated organic polymeric materials for photocatalytic CO_2 conversion," *Nanoscale*, vol. 14, no. 41, pp. 15217–15241, Jan. 2022, doi: 10.1039/d2nr04727f.

[32] M. D. Purkayastha, S. Denrah, N. Singh, M. Sarkar, G. K. Darbha, and T. P. Majumder, "Crystal structure dependent photocatalytic degradation of manganese and titanium oxides composites," *SN Applied Sciences*, vol. 2, no. 6, May 2020, doi: 10.1007/s42452-020-2933-7.

[33] P. Venkatesan, P. Kumari, and N. Remya, "Solar photocatalytic degradation of metformin by TiO_2 synthesized using *Calotropis gigantea* leaf extract," *Water Science and Technology*, vol. 83, no. 5, pp. 1072–1084, Feb. 2021, doi: 10.2166/wst.2021.040.

[34] W. Lin, X. Zhang, P. Li, Y. Tan, and Y. Ren, "Ultraviolet photolysis of metformin: Mechanisms of environmental factors, identification of intermediates, and density functional theory calculations," *Environmental Science and Pollution Research*, vol. 27, no. 14, pp. 17043–17053, Mar. 2020, doi: 10.1007/s11356-020-08255-9.

[35] S. Abbasi, "Improvement of photocatalytic decomposition of methyl orange by modified MWCNTs, prediction of degradation rate using statistical models," *Journal of Materials Science: Materials in Electronics*, vol. 32, no. 11, pp. 14137–14148, May 2021, doi: 10.1007/s10854-021-05707-x.

[36] A. Rafiq, M. Ikram, S. Ali, F. Niaz, M. Khan, Q. Khan, and M. Maqbool, "Photocatalytic degradation of dyes using semiconductor photocatalysts to clean industrial water pollution," *Journal of Industrial and Engineering Chemistry*, vol. 97, pp. 111–128, May 2021, doi: 10.1016/j.jiec.2021.02.017.